The Astrophysical Journal Letters, 829:L22 (6pp), 2016 October 1 doi:10.3847/2041-8205/829/2/L22

STRONGER REFLECTION FROM BLACK HOLE ACCRETION DISKS IN SOFT X-RAY STATES

James F. Steiner[1,3], Ronald A. Remillard[1], Javier A. García[2], and Jeffrey E. McClintock[2]
[1] MIT Kavli Institute for Astrophysics and Space Research, MIT, 70 Vassar Street, Cambridge, MA 02139, USA; jsteiner@mit.edu
[2] Harvard-Smithsonian Center for Astrophysics, 60 Garden Street, Cambridge, MA 02138, USA
Received 2016 August 12; revised 2016 September 9; accepted 2016 September 12; published 2016 September 22

ABSTRACT

We analyze 15,000 spectra of 29 stellar-mass black hole (BH) candidates collected over the 16 year mission lifetime of *Rossi X-ray Timing Explorer* using a simple phenomenological model. As these BHs vary widely in luminosity and progress through a sequence of spectral states, which we broadly refer to as hard and soft, we focus on two spectral components: the Compton power law and the reflection spectrum it generates by illuminating the accretion disk. Our proxy for the strength of reflection is the equivalent width of the Fe–K line as measured with respect to the power law. A key distinction of our work is that for *all* states we estimate the continuum under the line by excluding the thermal disk component and using only the component that is responsible for fluorescing the Fe–K line, namely, the Compton power law. We find that reflection is several times more pronounced (∼3) in soft compared to hard spectral states. This is most readily caused by the dilution of the Fe line amplitude from Compton scattering in the corona, which has a higher optical depth in hard states. Alternatively, this could be explained by a more compact corona in soft (compared to hard) states, which would result in a higher reflection fraction.

Key words: accretion, accretion disks – black hole physics – X-rays: binaries

1. INTRODUCTION

During the course of its 16 year mission, the *Rossi X-ray Timing Explorer* (*RXTE*) detected far more photons (30 billion in PCU-2 alone) from accreting black holes (BHs) than any other X-ray observatory. The sample of BHs targeted by *RXTE* is chiefly comprised of nearby stellar-mass systems. While the total Galactic population of stellar BHs is believed to be many millions, only a tiny subset of approximately 50 are known to us, namely, those located in X-ray binaries.

A wondrous property of BHs, their utter simplicity, is the essence of the famous no-hair theorem: each BH in nature is fully described by just its mass and spin. Roughly half of the known stellar BHs have a dynamically determined mass. The measured masses range from ~5 to 20 $M_{\odot}$ (Özel et al. 2010; Reid et al. 2014; Laycock et al. 2015; Wu et al. 2016). Meanwhile, estimates of spin have been obtained for many of them during the past decade, principally by modeling either the thermal continuum emission of the accretion disk (e.g., Zhang et al. 1997; McClintock et al. 2014) or the relativistically broadened reflection spectrum (e.g., Fabian et al. 1989; Reynolds 2014).

Our focus is primarily on transient BH systems that cycle between a minuscule fraction of the Eddington limit upward to the limit itself. During an outburst, a transient BH progresses through a sequence of spectral-timing states, which are broadly termed "hard" or "soft," based on a measure of X-ray hardness (Fender et al. 2004). As a source evolves over the course of months and its hardness varies, sweeping changes occur in many properties of the system including the composition of its spectrum, the intensity of Fourier flicker noise, and the presence or absence of quasi-periodic oscillations and jets (e.g., Homan & Belloni 2005; Remillard & McClintock 2006; Heil et al. 2015).

Stellar BHs emit a complex multicomponent X-ray spectrum. A *thermal* blackbody-like component is produced in the very inner accretion disk. The disk is truncated at a radius $R_{\rm in}$ before reaching the event horizon. A hard *power-law* component results from Compton scattering of the thermal disk photons in hot coronal gas that veils the disk. The third principal component is a *reflection* spectrum generated by illumination of the cold disk ($kT \sim 0.1$–1 keV) by the power-law component. The reflection component is a rich mix of radiative recombination continua, absorption edges, and fluorescent lines (Ross & Fabian 1993; García & Kallman 2010). An analysis of these three interacting spectral components provides constraints on the source properties including geometry (e.g., on $R_{\rm in}$ and the scale of the corona). The relationships between these components across the full range of behavior displayed by accreting stellar BHs is the focus of this Letter.

Our results are based on an analysis for 29 stellar BHs (10 dynamically confirmed BHs and 19 BH candidates) of all the data collected using *RXTE*'s prime detector unit (PCU-2), some 15,000 spectra in all, with a total net exposure time of 30 Ms. Importantly, we recalibrate the data using our tool PCACORR, which greatly reduces the level of systematic error (García et al. 2014a). Given the scope of our study, relativistic reflection models are too complex and computationally slow for our purposes (e.g., `reflionx`, `xillver`, `relxill`; Ross & Fabian 2005; García et al. 2014b). We therefore employ a simplistic, phenomenological model and estimate the strength of the reflection spectrum by determining the equivalent width with respect to the Compton continuum of its most prominent reflection feature, namely, the 6.4–7.0 keV Fe–K line.

The Letter is organized as follows. In Section 2, we describe the data sample and our approach to modeling the data. Our results are presented in Section 3, followed by a discussion in Section 4 and our conclusions in Section 5.

2. DATA

The *RXTE* archive provides the premier database for the synoptic study of stellar BHs. We exclusively use the data collected by PCU-2, one of the five proportional counter detectors that comprise *RXTE*'s principal instrument, the

[3] Einstein Fellow.

Table 1
RXTE's PCU-2 BH Archive

System	R.A.	Decl.	N_{obs}	T_{obs} (ks)	PCU-2 Counts (10^6)	N_H (10^{22} cm^{-2})	References
LMC X-3	05 38 56.3	−64 05 03	704	1203.95	33.5	0.04	(1)
LMC X-1	05 39 38.8	−69 44 36	1598	3120.72	106.4	0.7	(2)
XTE J1118+480	11 18 10.8	+48 02 13	124	220.93	15.7	0.01	(3)
GS 1354-64	13 58 09.9	−64 44 05	23	54.46	6.2	2	(4)
4U 1543-47	15 47 08.6	−47 40 10	130	243.26	278.2	0.4	(3)
XTE J1550–564	15 50 58.8	−56 28 35	517	970.78	1875.6	0.8	(5)
4U 1630-47[a]	16 34 01.6	−47 23 35	1194	2108.10	1034.0	11	(6)
XTE J1650-500	16 50 01.0	−49 57 44	195	337.28	119.5	0.5	(3)
XTE J1652-453	16 52 20.3	−45 20 40	61	99.84	9.2	6.7	(7)
GRO J1655-40	16 54 00.1	−39 50 45	987	2483.87	5174.2	0.7	(3)
MAXI J1659-152	16 59 01.7	−15 15 29	71	146.64	66.7	0.25	(8)
GX 339-4	17 02 49.4	−48 47 23	1672	2868.46	894.2	0.3	(9)
IGR J17091-3624	17 09 08	−36 24.4	256	479.60	46.8	1.2	(10)
XTE J1720-318	17 19 59.0	−31 45 01	122	283.36	80.7	1.3	(4)
GRS 1739-278	17 42 40.0	−27 44 53	12	26.45	15.2	3.7	(4)
H1743-322	17 46 15.6	−32 14 01	649	1403.18	958.5	2.2	(11)
XTE J1748-288	17 48 05.1	−28 28 26	39	98.58	46.6	7.5	(4)
SLX 1746-331	17 49 48.3	−33 12 26	78	186.19	36.2	0.4	(3)
XTE J1752-223	17 52 15.1	−22 20 33	234	435.52	147.0	0.6	(12)
Swift J1753.5-0127	17 53 28.3	−01 27 06	376	853.95	123.4	0.15	(3)
XTE J1817-330	18 17 43.5	−33 01 08	191	430.11	270.7	0.15	(4)
XTE J1818-245	18 18 24.4	−24 32 18	56	141.74	19.7	0.5	(13)
V4641 Sgr	18 19 21.6	−25 24 26	94	179.57	3.0	0.25	(3)
MAXI J1836-194	18 35 43.4	−19 19 12	76	124.83	9.4	0.15	(3)
XTE J1859+226	18 58 41.6	+22 39 29	170	336.24	270.3	0.2	(14)
GRS 1915+105	19 15 11.6	+10 56 45	2566	5255.58	12520.1	6	(15)
Cyg X-1	19 58 21.7	+35 12 06	2446	5413.02	6361.3	0.7	(3)
4U 1957+115	19 59 24.2	+11 42 32	243	646.42	41.0	0.15	(3)
XTE J2012+381	20 12 37.7	+38 11 01	30	53.98	13.5	1.3	(4)
Total	...	...	14914	30207.	30577.	...	...

Note.
[a] For 76 observations the source was offset in the 1° FWHM collimator by ∼0.°6, which significantly reduced the count rate. No other source has more than several pointings offset by >0.°5.
References. (1) Steiner et al. (2010), (2) Gou et al. (2009), (3) Dickey & Lockman (1990), (4) Dunn et al. (2010), (5) Steiner et al. (2011), (6) Tomsick et al. (2005), (7) Hiemstra et al. (2011), (8) Yamaoka et al. (2012), (9) Hynes et al. (2004), (10) Rodriguez et al. (2011), (11) McClintock et al. (2009), (12) Nakahira et al. (2012), (13) Cadolle Bel et al. (2009), (14) Farinelli et al. (2013), (15) Feroci et al. (1999).

Proportional Counter Array (PCA). Throughout the mission, PCU-2 was the unit that was most often active, and it had the most reliable and stable calibration (Jahoda et al. 2006; Shaposhnikov et al. 2012). Its area and energy resolution were 1300 cm^2 and ≈18% at 6 keV. Table 1 summarizes our data sample.

During an outburst, a BH was typically observed daily over a period of months as it systematically brightened and subsequently dimmed by orders of magnitude. We homogenized the data by segmenting it into continuous 300–5000 s intervals, each of which was used to produce an energy spectrum and a power-density spectrum (PDS). Energy spectra were analyzed ignoring the lowest four channels, an effective lower bound ≈2.8 keV, and an upper bound of 45 keV was adopted. The effects of detector dead time were corrected as described in McClintock et al. (2006). We obtained an absolute calibration of the flux using the the standard Toor & Seward (1974) spectrum of the Crab Nebula; our slope and normalization corrections are $\Delta\Gamma = 0.01$ and $f_{TS} = 1.097$ (Steiner et al. 2010). We computed the rms power, a measure of the flicker noise, by integrating the PDS over the band 0.1–10 Hz.

An unprecedented sensitivity to faint spectral features is achieved by employing the calibration tool PCACORR (García et al. 2014a), which improves the quality of the PCA's spectral calibration by roughly an order of magnitude and results in a data precision of ∼0.1%. We include this small systematic uncertainty as a fractional error on each channel when conducting our analysis using XSPEC (Arnaud 1996). The considerable increase in sensitivity PCACORR delivers is crucial for estimating the strength of line features.

All PCU-2 data for 29 BHs are plotted in a hardness–intensity diagram (HID; Fender et al. 2004; Remillard & McClintock 2006) in the top panel of Figure 1. The normalized hard color (or hardness ratio HR) is the ratio of count rates in the energy bands indicated in the upper panel and is described in Peris et al. (2016). The data are color-coded to show the level of rms flicker noise. As is well known and evident here from the vertical striation, rms noise correlates with spectral state (e.g., Remillard & McClintock 2006; Heil et al. 2015), with hard states showing several times stronger rms than soft states. The six small panels are HIDs for selected sources. Note that transient sources characteristically trace a loop in the HID, but that the persistent source Cyg X–1 is confined to a

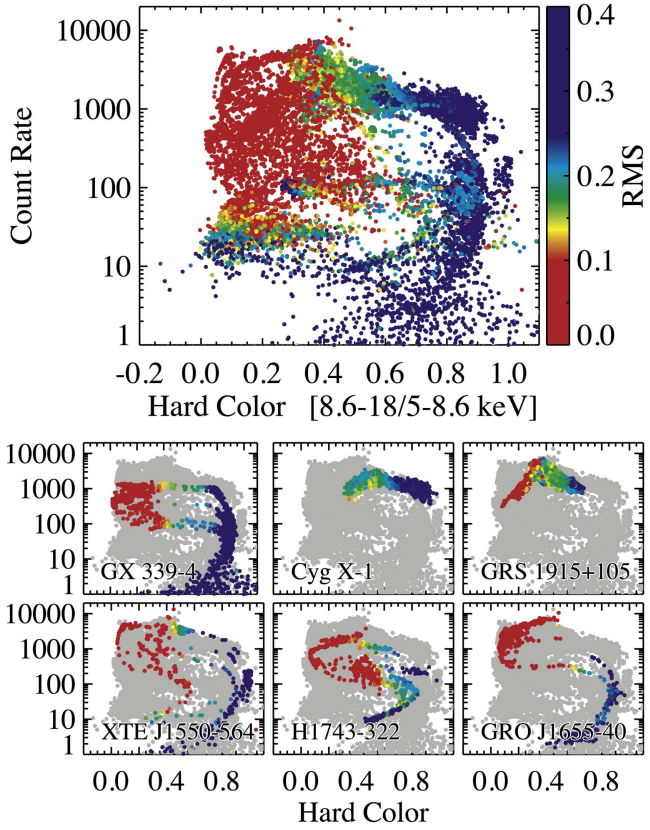

Figure 1. (top) Hardness–intensity diagrams for all data and (bottom) for six well-known BHs with abundant data (where for reference the gray background shows all data). For reference, the count rate of the Crab Nebula is ≈2600 s^{-1}. Note that an HID does not allow one to compare the luminosities of sources because the intensity is in detector units.

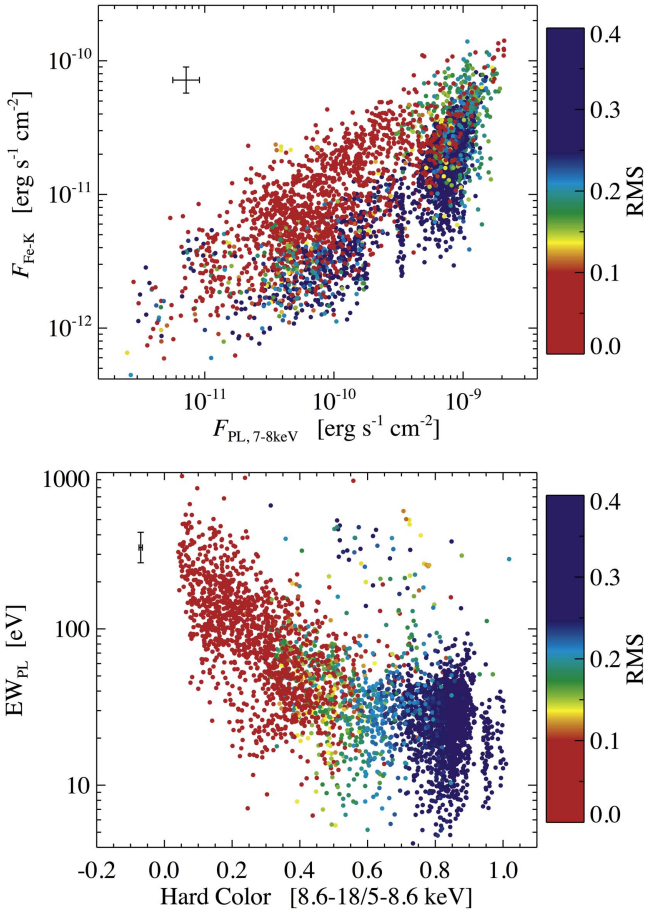

Figure 2. (top) Flux in the Fe line vs. the adjacent flux in the power-law continuum. Color-mapping indicates the rms power. (bottom) Equivalent width of the Fe line computed using the power-law flux only (i.e., excluding the disk flux). The reflection is strongest in soft states, and it increases dramatically as the spectrum softens. Representative 1σ error bars are shown in the upper left corner in each panel.

relatively narrow region. The other selected source showing stunted HID evolution is GRS 1915+105, which is an unusual transient system that has been in a protracted state of outburst since 1992.

2.1. Spectral Modeling

We adopt a single simplistic spectral model that is applicable to both soft and hard spectra: `phabs*[smedge(simpl⊗-diskbb)+Gauss]`. The disk and Compton components are modeled by `diskbb` (Mitsuda et al. 1984) and `simpl` (Steiner et al. 2009), respectively. The reflection component is described by a Gaussian line with fixed energy of 6.5 keV and an intrinsic width of 50 eV. We note that owing to the broad detector resolution at the Fe line ∼1.2 keV, the value adopted for the line width in our simplistic model is of minor consequence (as demonstrated in Section 4). Despite its coarse resolution, *RXTE* is very sensitive to the line flux, as measured by the normalization of the Gaussian feature. Accordingly, we adopt the line flux as our proxy for the intensity of the reflection component. We approximate the relativistically broadened Fe–K absorption edge using `smedge` (Ebisawa et al. 1994); we fit for the peak depth $\tau_{\rm smedge}$ with the width fixed at 7 keV and the shape index set to −2.67 (Sobczak et al. 2000). Our adopted values of the column density $N_{\rm H}$ are summarized in Table 1.

3. RESULTS

We have fitted all ≈15,000 spectra with our model. In Figure 2, results are shown for approximately one-quarter of these spectra, those that meet three criteria: $\chi^2/\nu < 2$; Fe-line normalization significant at the $\geqslant 1\sigma$ level; and power-law normalization $f_{\rm SC}$ significant at the $\geqslant 3\sigma$ level. Plotted in the top panel is Gaussian line flux versus the Compton power law flux near the Fe edge computed by integrating the power-law component from 7 to 8 keV. Since the fluorescent Fe K line is produced preferentially by photons at energies above and near the Fe K edge (Reynolds et al. 2009), i.e., at energies $E \gtrsim 7$ keV (Kallman et al. 2004), it is not surprising that the line and continuum fluxes are strongly correlated. Though notably, this strong correlation is a direct validation of the reflection paradigm (wherein power-law emission fluoresces strong line emission). What is surprising is that the soft states (red) appear to be much more efficient at producing reflection than hard states (blue), as evidenced by the vertical offset between the clouds of soft and hard data.

This result runs counter to the conventional view that reflection is weak in soft states (e.g., Ross & Fabian 2007; Yuan & Narayan 2014; but see the correlation between spectral index and reflection strength in Zdziarski et al. 1999 and related work), a view based on the weakness of reflection *relative to*

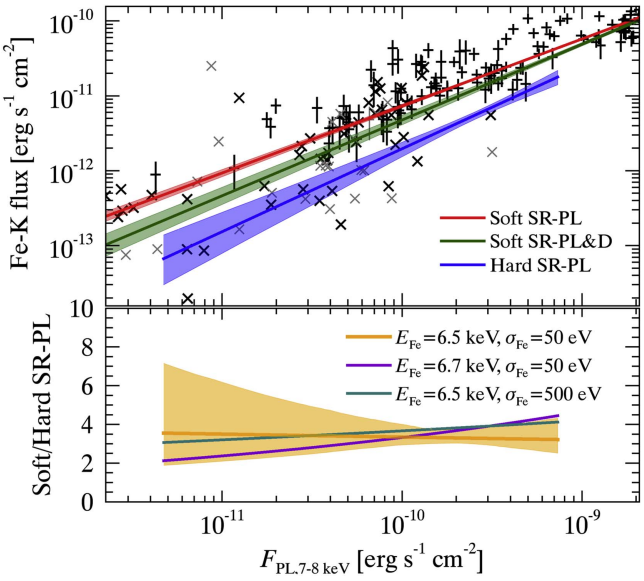

Figure 3. (top) Fe-line flux vs. 7–8 keV power-law flux for J1550. Our primary "SR-PL" scaling relation is shown in red with its associated 95% confidence region. The "SR-PL&D" curve in green includes the effects of returning radiation. For reference, the SR-PL fit to the hard data is shown in blue. At this level of detail, only those data with total flux >3 mCrab and that yielded fits with $\chi^2/\nu < 2$ are shown. For clarity, data are marked with crosses and error bars omitted when $|N_{\rm line}|/\sigma_{\rm line} < 2$. Data consistent with absorption (i.e., $N_{\rm line} < 0$) are plotted in gray. (bottom) Ratio of the Fe-line flux for soft states to that for hard states computed using the SR-PL scaling relation. Our default curve is presented in orange with its associated 95% confidence intervals as a lightly shaded region. Results for alternate spectral models with different values of the Gaussian line energy and line width, which produce modest systematic differences, are also shown for comparison.

the thermal disk component. Here, instead, we appropriately relate the strength of the reflection signal to the power-law component that produces it, as isolated from the evolving thermal disk.

In the lower panel of Figure 2, we plot (versus the hardness ratio HR) our proxy for the strength of reflection: i.e., we plot the equivalent width ($\rm EW_{PL}$) of the line with respect to the coronal flux. That reflection that is more pronounced for soft states is readily apparent. In soft states, $\rm EW_{PL}$ decreases regularly by an order of magnitude as the spectrum hardens; then, for intermediate and hard states it plateaus at HR $\gtrsim 0.7$. Given the inhomogeneity of our data sample, which includes both transient and persistent sources, the ordered quality of these data is striking.

3.1. A Case Study in Reflection: XTE J1550–564

To more precisely study the behavior of reflection in soft spectral states, we examine one system in detail. We select an exceptionally bright transient with abundant data: XTE J1550–564 (hereafter J1550; see the bottom left subpanel of Figure 1). J1550 was discovered on 1998 September 6, and two weeks later it reached a peak intensity of 6.8 Crab (2–10 keV). Four additional fainter outbursts were observed during the following decade.

We define HR = 0.7 as the cut between soft and hard state data, and we again (as in Figure 2) examine the relationship between our proxy for reflection (namely, the flux in the Fe K line) and the flux in the adjacent Compton continuum. The data are plotted in Figure 3. We begin with a simplistic assumption that the coronal flux and Fe line flux will scale together, i.e., $F_{\rm Fe} \equiv \alpha F^{\beta}_{\rm PL,7-8\,keV}$, and we proceed to fit for α and β. This *scaling relation* is termed SR-PL to emphasize that the line flux scales with the power law. We likewise pursue the SR-PL fit for hard spectra (i.e., HR > 0.7), with the constants of soft and hard data determined independently.

For the soft data, we additionally investigate the possibility that disk self-irradiation may also contribute to the reflection emission. This is a motivated notion given that bright soft states can produce appreciable thermal emission even above 5 keV, and, further, some fraction of the thermal photons (the "returning radiation") is bent back and strikes the disk rather than escaping to infinity. We consider returning radiation by allowing for an added scaling with the disk's emission in the same 7–8 keV band proximate to the Fe–K edge, i.e., $F_{\rm Fe} \equiv \alpha F^{\beta}_{\rm PL,7-8\,keV} + \gamma F^{\delta}_{\rm disk,7-8\,keV}$ (this is the SR-PL&D scaling relation), and we likewise fit for its parameters.

In the top panel of Figure 3, we show the Compton component's contribution to the Fe-line flux for both the SR-PL (red) and SR-PL&D (green) fits. The contribution to the line flux from returning radiation is vanishingly small, particularly at the highest luminosities. In the same figure, for reference we also show the SR-PL fit to the hard data in blue. Note that the error bounds for both soft-data fits lie well above the hard correlation bounds.

The best-fitting scale indexes and 1σ errors are $\beta_{\rm SR-PL,soft} = 0.90 \pm 0.01$, $\beta_{\rm SR-PL,hard} = 1.12 \pm 0.12$ and $\beta_{\rm SR-PL\&D,soft} = 1.01 \pm 0.03$, $\delta_{\rm SR-PL\&D,soft} = 0.43 \pm 0.03$. The SR-PL&D fit slightly outperformed the SR-PL fit ($\Delta\chi^2 \approx 20$ for 2 added degrees of freedom).

Having established that the effects of returning radiation are minor, we focus on comparing reflection for soft and hard data using solely the SR-PL curves. We produce Markov Chain Monte Carlo realizations for both the hard and soft SR-PL correlations (top panel of Figure 3), and we compare their respective Fe-line fluxes. The results are shown in the bottom panel of Figure 3. On average, the Fe line is >3 times stronger for soft data, while the 95% confidence region ranges from ~2 to 9 times stronger.

4. DISCUSSION

As illustrated in Figure 3, our estimate of the ratio of the Fe-line flux in soft and hard states is only modestly sensitive to the values we adopted for the line energy (6.5 keV) and width (50 eV). Varying these values does not affect our conclusions. We have also explored other model formulations (e.g., including a power-law cutoff and replacing the Gaussian by a relativistic line profile) and have similarly found that our conclusions are unaffected. Varying the line shape systematically rescales the line flux, but it has a minor affect on the ratio of the fluxes in soft and hard states, which is our focus.

Consideration of two shortcomings of our simplistic model serves to strengthen our conclusion that soft states are more efficient in producing reflection emission. First, soft-state disks are hotter and more strongly ionized, and hence they generally produce more reflection continuum emission, which gets lumped together with the Compton power law. In the case of our simple model, this effect serves to boost the power-law continuum, thereby reducing $\rm EW_{PL}$ for the soft state. Second, Fe-line absorption features in disk winds are preferentially and often observed in soft states (Ponti et al. 2012), and these absorption features act to weaken the emission line. Our finding of enhanced $\rm EW_{PL}$ in soft states is thus contrary to these biases.

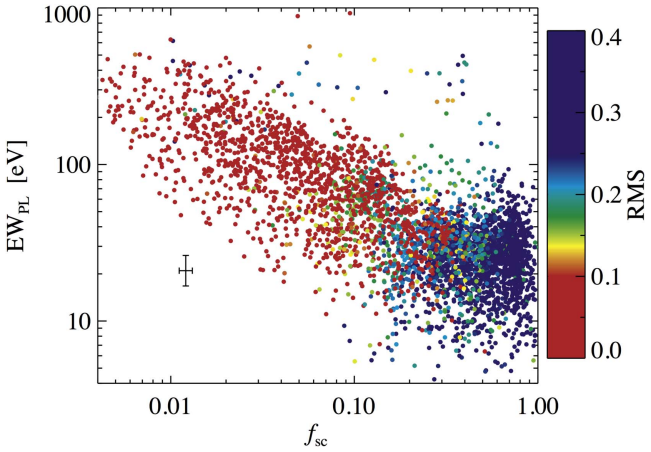

Figure 4. Strong anti-correlation between f_{SC} and EW_{PL}, as predicted by Petrucci et al. (2001). The dilution of line flux by Compton scattering of varying optical depth naturally accounts for the more pronounced EW_{PL} in soft states.

Earlier work by Petrucci et al. (2001) that examined the effect of Comptonizing reflection spectra showed that at a fixed value of Γ, the fitted Fe–K equivalent width is very sensitive to the coronal temperature kT_e, principally because as kT_e decreases, optical depth τ necessarily increases (a straightforward consequence of the equations governing thermal Comptonization). Accordingly, at high optical depth, the line is highly scattered in the corona. The scattered portion blends with the continuum, which results in a decrease in the Gaussian's equivalent width. We have examined the evolution of equivalent width versus spectral hardness (changing Γ) and other spectral parameters. There is a strong anti-correlation between f_{SC} and EW_{PL} in precisely the sense predicted by Petrucci et al. (2001), and is the most apparent explanation for the observed trend. This is shown in Figure 4.

Alternatively, or in addition to the dilution of the line by Compton scattering in the corona, changes in the disk-coronal geometry can impact the reflection's strength. In particular, a corona at very small scale-height (h_{corona}) coupled with a close-in disk yields a higher reflection fraction than when either (1) the disk is truncated or (2) the corona is very large compared to the event horizon (Dauser et al. 2014). Gradual evolution of accretion flow with more compact disk-coronal geometry (i.e., lower h_{corona}/R_{in}) in soft states would similarly contribute to the observed correlation.

We caution that the role of ionization is complex and varies nonlinearly as other coronal attributes change, including, most notably, Γ. These differences are principally related to changes in the atmosphere's temperature structure. For the range of ionization parameters observed around active stellar-mass BHs, i.e., $\log \xi \approx 2$–4, we simulated PCU-2 data using the XILLVER reflection model (García & Kallman 2010), and applied our analysis method. We found that EW_{PL} varies by a factor of $\sim$2–3 over the span of Γ (1.4–3.4) and ξ; this is insufficient to account for the full trend in Figure 2. Moreover, for $\log \xi \leqslant 3$, higher Γ tends to produce lower EW_{PL}, whereas at $\log \xi \gtrsim 3$, the trend reverses.

As summarized by Zdziarski et al. (2003), and also Gilfanov & Merloni (2014), there is abundant evidence for a strong positive correlation between spectral index and reflection strength (the "$R - \Gamma$" correlation). This has been seen in both BH X-ray binaries and in active galactic nuclei. However, such work has been largely confined to examination of hard states. To our knowledge, our work is the first compelling evidence that the correlation between spectral softness (increasing Γ) and reflection fraction continues and is strongly amplified in soft, thermal states (i.e., $\Gamma \sim$ 2–3). Further, from considering the *RXTE* archive of active BHs, as is readily apparent in Figure 2, this change is gradual and orderly among the full cast of stellar BHs.

5. CONCLUSIONS

We have examined the strength of reflection in a global study of stellar BHs using a simplistic, phenomenological spectral model. We directly validate the reflection paradigm, wherein power-law flux induces reflection emission. In separating possible contribution from disk self-irradiation, we demonstrate that the power law's contribution is dominant.

Most importantly, we show that the corona produces reflection features up to an order of magnitude more pronounced in soft rather than hard states. The data suggest an ordered transition in which the line-to-continuum strength declines gradually with spectral hardness. This is the first time the "$R - \Gamma$" correlation has been shown to extend through (and increase in) BH soft states. One possible explanation is that a more compact disk-coronal geometry in soft states would produce the observed trend. However, the most natural explanation for this trend is suggested by Petrucci et al. (2001), who describe the dilution of line features emitted by the disk due to Compton scattering in the corona. In our case, because hard states have corona with higher optical depth than soft states, their line features are correspondingly weakened resulting in the observed anti-correlation between HR and reflection strength.

J.F.S. has been supported by the NASA Einstein Fellowship grant PF5-160144.

Facility: RXTE.

REFERENCES

Arnaud, K. A. 1996, in ASP Conf. Ser. 101, Astronomical Data Analysis Software and Systems V, ed. G. H. Jacoby & J. Barnes (San Francisco, CA: ASP), 17
Cadolle Bel, M., Prat, L., Rodriguez, J., et al. 2009, A&A, 501, 1
Dauser, T., García, J., Parker, M. L., Fabian, A. C., & Wilms, J. 2014, MNRAS, 444, L100
Dickey, J. M., & Lockman, F. J. 1990, ARA&A, 28, 215
Dunn, R. J. H., Fender, R. P., Körding, E. G., Belloni, T., & Cabanac, C. 2010, MNRAS, 403, 61
Ebisawa, K., Ogawa, M., Aoki, T., et al. 1994, PASJ, 46, 375
Fabian, A. C., Rees, M. J., Stella, L., & White, N. E. 1989, MNRAS, 238, 729
Farinelli, R., Amati, L., Shaposhnikov, N., et al. 2013, MNRAS, 428, 3295
Fender, R. P., Belloni, T. M., & Gallo, E. 2004, MNRAS, 355, 1105
Feroci, M., Matt, G., Pooley, G., et al. 1999, A&A, 351, 985
García, J., Dauser, T., Lohfink, A., et al. 2014b, ApJ, 782, 76
García, J., & Kallman, T. R. 2010, ApJ, 718, 695
García, J. A., McClintock, J. E., Steiner, J. F., Remillard, R. A., & Grinberg, V. 2014a, ApJ, 794, 73
Gilfanov, M., & Merloni, A. 2014, SSRv, 183, 121
Gou, L. J., McClintock, J. E., Liu, J., et al. 2009, ApJ, 701, 1076
Heil, L. M., Uttley, P., & Klein-Wolt, M. 2015, MNRAS, 448, 3339
Hiemstra, B., Méndez, M., Done, C., et al. 2011, MNRAS, 411, 137
Homan, J., & Belloni, T. 2005, Ap&SS, 300, 107
Hynes, R. I., Steeghs, D., Casares, J., Charles, P. A., & O'Brien, K. 2004, ApJ, 609, 317
Jahoda, K., Markwardt, C. B., Radeva, Y., et al. 2006, ApJS, 163, 401
Kallman, T. R., Palmeri, P., Bautista, M. A., Mendoza, C., & Krolik, J. H. 2004, ApJS, 155, 675

Laycock, S. G. T., Cappallo, R. C., & Moro, M. J. 2015, MNRAS, 446, 1399
McClintock, J. E., Narayan, R., & Steiner, J. F. 2014, SSRv, 183, 295
McClintock, J. E., Remillard, R. A., Rupen, M. P., et al. 2009, ApJ, 698, 1398
McClintock, J. E., Shafee, R., Narayan, R., et al. 2006, ApJ, 652, 518
Mitsuda, K., Inoue, H., Koyama, K., et al. 1984, PASJ, 36, 741
Nakahira, S., Koyama, S., Ueda, Y., et al. 2012, PASJ, 64, 13
Özel, F., Psaltis, D., Narayan, R., & McClintock, J. E. 2010, ApJ, 725, 1918
Peris, C. S., Remillard, R. A., Steiner, J. F., et al. 2016, ApJ, 822, 60
Petrucci, P. O., Merloni, A., Fabian, A., Haardt, F., & Gallo, E. 2001, MNRAS, 328, 501
Ponti, G., Fender, R. P., Begelman, M. C., et al. 2012, MNRAS, 422, 11
Reid, M. J., McClintock, J. E., Steiner, J. F., et al. 2014, ApJ, 796, 2
Remillard, R. A., & McClintock, J. E. 2006, ARA&A, 44, 49
Reynolds, C. S. 2014, SSRv, 183, 277
Reynolds, C. S., Fabian, A. C., Brenneman, L. W., et al. 2009, MNRAS, 397, L21
Rodriguez, J., Corbel, S., Caballero, I., et al. 2011, A&A, 533, L4
Ross, R. R., & Fabian, A. C. 1993, MNRAS, 261, 74
Ross, R. R., & Fabian, A. C. 2005, MNRAS, 358, 211
Ross, R. R., & Fabian, A. C. 2007, MNRAS, 381, 1697
Shaposhnikov, N., Jahoda, K., Markwardt, C., Swank, J., & Strohmayer, T. 2012, ApJ, 757, 159
Sobczak, G. J., McClintock, J. E., Remillard, R. A., et al. 2000, ApJ, 544, 993
Steiner, J. F., McClintock, J. E., Remillard, R. A., et al. 2010, ApJL, 718, L117
Steiner, J. F., McClintock, J. E., Remillard, R. A., et al. 2011, MNRAS, 416, 941
Steiner, J. F., Narayan, R., McClintock, J. E., & Ebisawa, K. 2009, PASP, 121, 1279
Tomsick, J. A., Corbel, S., Goldwurm, A., & Kaaret, P. 2005, ApJ, 630, 413
Toor, A., & Seward, F. D. 1974, AJ, 79, 995
Wu, J., Orosz, J. A., McClintock, J. E., et al. 2016, ApJ, 825, 46
Yamaoka, K., Allured, R., Kaaret, P., et al. 2012, PASJ, 64, 32
Yuan, F., & Narayan, R. 2014, ARA&A, 52, 529
Zdziarski, A. A., Lubiński, P., Gilfanov, M., & Revnivtsev, M. 2003, MNRAS, 342, 355
Zdziarski, A. A., Lubiński, P., & Smith, D. A. 1999, MNRAS, 303, L11
Zhang, S. N., Cui, W., & Chen, W. 1997, ApJL, 482, L155